Inorg. Chem. **2004**, *43*, 8361–8366

Unique Hydrogen Bonding Correlating with a Reduced Band Gap and Phase Transition in the Hybrid Perovskites $(HO(CH_2)_2NH_3)_2PbX_4$ (X = I, Br)

Nicolas Mercier,* Sylvain Poiroux, Amédée Riou, and Patrick Batail

Laboratoire de Chimie, Ingénierie Moléculaire et Matériaux d'Angers, UMR-CNRS 6200, Université d'Angers 2 Bd Lavoisier, 49045 Angers, France

Received August 26, 2004

The first hybrid perovskites incorporating alcohol-based bifunctional ammonium cations, $(HO(CH_2)_2NH_3)_2PbX_4$ (X = I, Br), have been prepared and characterized. $(HO(CH_2)_2NH_3)_2PbI_4$ adopts a monoclinic cell, $a = 8.935(1)$ Å, $b = 9.056(2)$ Å, $c = 10.214(3)$ Å, $\beta = 100.26(1)°$, $V = 813.3(3)$ Å^3, $P2_1/a$, and $Z = 2$, and $(HO(CH_2)_2NH_3)_2PbBr_4$ is orthorhombic, $a = 8.4625(6)$ Å, $b = 8.647(1)$ Å, $c = 19.918(2)$ Å, $V = 1457.5(2)$ Å^3, *Pbcn*, and $Z = 4$. In the layered structures, a unique hydrogen-bond network connects adjacent perovskite layers, owing to OH····X, NH_3^+····X, and intermolecular NH_3^+···OH interactions. Its impact on the bonding features of the inorganic framework and on the quite short interlayer distance, in the case of $(HO(CH_2)_2NH_3)_2PbI_4$, is shown. As a result, a significant red shift of the exciton peaks ($\lambda = 536$ nm (X = I), $\lambda = 417$ nm (X = Br)), compared to other PbX_4^{2-}-based perovskite hybrids, is observed, revealing a reduced band gap. A reversible structural transition occurs at $T = 96$ °C (X = I) and $T = 125$ °C (X = Br). An orthorhombic cell of the high-temperature phase of $(HO(CH_2)_2NH_3)_2PbI_4$ with $a_{HT} = 18.567(6)$ Å, $b_{HT} = 13.833(6)$ Å, $c_{HT} = 6.437(2)$ Å, and $V = 1653$ Å^3 is proposed from powder X-ray diffraction. A change in the hydrogen bonding occurs, with molecules standing up in the interlayer space and OH parts probably interacting together, leading to a more conventional situation for ammonium groups and a more distorted perovskite layer. This is in accordance with the blue shift of the exciton peak to $\lambda = 505$ nm (X = I) or to $\lambda = 374$ nm (X = Br) during the phase transition.

Introduction

Hybrid perovskites consist of perovskite layers alternating with organic sheets, the most common general formulas being $(RNH_3)_2M^{II}X_4$ or $(NH_3RNH_3)M^{II}X_4$ (M = Pb, Sn, Cu, ...; X = I, Br, Cl; R = alkyl, phenyl, thiophene derivatives, ...).[1] They received a considerable interest due to the opportunity to combine useful properties of the two components,[2−4] as for instance the possible solution processing of these hybrids by room-temperature techniques such as spin-coating. An extensive work has been recently devoted to semiconductive materials based on iodostannate perovskite layers, used as a semiconducting channel in thin-film field-effect transistor (TFTs).[4,5] A high charge carrier mobility was observed (0.6 cm^2 V^{-1} s^{-1}) in $(C_6H_5C_2H_5NH_3)_2SnI_4$,[5] which nevertheless remains 2 orders of magnitude smaller than in $CH_3NH_3SnI_3$, a 3D perovskite with metallic conductivity.[6] To improve this charge carrier mobility by tuning the electronic structure of semiconducting sheets, several strategies have been considered, including the synthesis of hybrids with enhanced structural dimensionality, either multilayer perovskite materials[5,7] or materials with perovskite monolayers linked by covalent bridges.[8] Also, the band gap can

* Author to whom correspondence should be addressed. E-mail: nicolas.mercier@univ-angers.fr. Tel.: 33.(2).41.73.50.83. Fax: 33.(2).41.73.54.05.

(1) Mitzi, D. B. *Prog. Inorg. Chem.* **1999**, *48*, 1−121.
(2) (a) Era, M.; Morimoto, S.; Tsutsui, T.; Saito, A. *Appl. Phys. Lett.* **1994**, *65*, 676. (b) Papavassiliou, G. C.; Mousdis, G. A.; Koutselas, I. B. *Adv. Mater. Opt. Electron.* **1999**, *9*, 265. (c) Papavassiliou, G. C.; Mousdis, G. A.; Koutselas, I. B. *Synth. Met.* **2001**, *121*, 1339.
(3) Mitzi, D. B.; Feild, C. A.; Harrison, W. T.; Guloy, A. M. *Nature* **1994**, *369*, 467.
(4) Mitzi, D. B.; Chondroudis, K.; Kagan, C. R. *IBM J. Res. Dev.* **2001**, *45* (1).
(5) Kagan, C. R.; Mitzi, D. B.; Chondroudis, K. *Sciences* **1999**, *286*, 945.
(6) Mitzi, D. B.; Field, C. A.; Schlesinger, Z.; Laibowitz, R. B. *J. Solid State Chem.* **1995**, *114*, 159.
(7) (a) Calabrese, J.; Jones, N. L.; Harlow, R. L.; Herron, N.; Thorn, D. L.; Wang, Y. *J. Am. Chem. Soc.* **1991**, *113*, 2328. (b) Zhu, X. H.; Mercier, N.; Riou, A.; Blanchard, P.; Frère, P. *Chem. Commun.* **2002**, *18*, 2160. (c) Xu, Z.; Mizi, D. B. *Inorg. Chem.* **2003**, *42*, 6589.

10.1021/ic048814u CCC: $27.50
Published on Web 11/24/2004

be modified by incorporating selected cations, which may influence the bonding features of the inorganic frameworks, essentially due to steric interactions in organics sheets.[9−11] In this way, the use of primary ammonium cations also bearing a hydrogen donor/acceptor part certainly would more strongly influence the organization of both organic and inorganic parts in hybrids.

Herein, we report the preparation, the X-ray structural characterization, and the optical absorption spectra of the first organic−inorganic hybrid perovskites incorporating an alcohol-based bifunctional ammonium cation, $(HO(CH_2)_2NH_3)_2PbX_4$ (X = I, Br). In the structures, hydrogen-bonded self-assembled pairs of ammonium cations occur and couple the adjacent perovskite layers, which also appear only slightly distorted. Remarkably, these structural features involve a significant reduced band gap, as expressed by a red shift of the exciton peak. A reversible structural transition observed at 96 °C in $HO(CH_2)_2NH_3)_2PbI_4$ and at 125 °C in $HO(CH_2)_2NH_3)_2PbBr_4$ will be also discussed, from powder X-ray diffraction experiments, thermal analysis, and optical absorption spectra. A change of the hydrogen bonding including ammonium groups is proposed to explain the significant blue shift of the exciton peak of the high-temperature phase, illustrating the possibility with such cations to substantially tune the electronic properties as the temperature changes.

Experimental Section

Synthesis. $(HO(CH_2)_2NH_3)_2PbI_4$ was formed from a mixture of $NH_2(CH_2)_2OH$ (111 mg, 1.82 mmol), PbI_2 (420 mg, 0.91 mmol), a few drops of concentrated HI, and acetonitrile (20 mL), which was stirred a few minutes at room temperature, giving a clear yellow-brown solution. After evaporation (T = 20 °C) by stirring the solution, very thin platelike crystals of $(HO(CH_2)_2NH_3)_2PbI_4$ were formed. The intense orange crystals were collected by filtration and washed rapidly with cold acetonitrile. The same procedure, starting from $PbBr_2$ and HBr, lead to a pale yellow crystallized powder of $(HO(CH_2)_2NH_3)_2PbBr_4$. A powder X-ray pattern of the homogeneous samples showed that all reflections are indexed in the monoclinic cell of $(HO(CH_2)_2NH_3)_2PbI_4$ and the orthorhombic cell of $(HO(CH_2)_2NH_3)_2PbBr_4$ (Table 1), respectively (see Supporting Information). Crystals, with size up to 1 × 0.4 × 0.1 mm^3 for the biggest ones, could be obtained from a slow evaporation of acetonitrile over a period of 2 days.

X-ray Crystallography. X-ray diffraction data for selected single crystals were collected on an Enraf-Nonius MACH3 four-circle diffractometer for $(HO(CH_2)_2NH_3)_2PbI_4$ and on a Brucker-Nonius KAPPA-CDD diffractometer for $(HO(CH_2)_2NH_3)_2PbBr_4$, both using graphite-monochromated Mo Kα radiation (λ = 0.710 73 Å). A summary of crystallographic data and results of refinements are given in Table 1. Both structures were solved and refined using the Shelxl97 package. Heavy atoms (Pb, I, Br) were first located using direct methods, C, O, and N atoms being then located from the analysis of the Fourier difference maps. Hydrogen atoms were treated with a riding model, except for the hydrogen atom belonging to the hydroxyl group, which was located from the Fourier difference map, the C2−O−H8 bond angle being 112.5° in $(HO(CH_2)_2NH_3)_2PbI_4$ (see Figure 2a, below) and C2−O−H1 being 122.0° in $(HO(CH_2)_2NH_3)_2PbBr_4$. Positions and anisotropic thermal motion parameters of the non-H atoms were refined by full-matrix least-squares routines against F^2. Absorption effects were corrected using the Gauss method for $(HO(CH_2)_2NH_3)_2PbBr_4$ and an empirical method for $(HO(CH_2)_2NH_3)_2PbI_4$. Selected bond distances and angles for $(HO(CH_2)_2NH_3)_2PbI_4$ and $(HO(CH_2)_2NH_3)_2PbBr_4$ are provided in Tables 2 and 3. A complete list of crystallographic data, along with the atomic coordinates and the anisotropic motion parameters for each compound, is given as Supporting Information.

Room-temperature powder X-ray scans were performed on a Philips PW1050 diffractometer (copper Kα radiation), and the cell

Table 1. Crystallographic Data for $(HO(CH_2)_2NH_3)_2PbI_4$ and $(HO(CH_2)_2NH_3)_2PbBr_4$

	$(HO(CH_2)_2NH_3)_2PbI_4$	$(HO(CH_2)_2NH_3)_2PbBr_4$
empirical formula	$C_4H_{16}I_4N_2O_2Pb$	$C_4H_{16}Br_4N_2O_2Pb$
fw (g/mol)	838.98	651.00
cryst size (mm^3)	0.80 × 0.12 × 0.05	0.30 × 0.30 × 0.05
space group	$P2_1/a$	Pbcn
a, Å	8.935(1)	8.4625(6)
b, Å	9.056(2)	8.647(1)
c, Å	10.214(3)	19.918(2)
α, deg	90	90
β, deg	100.26(1)	90
γ, deg	90	90
V, Å^3	813.3(3)	1457.5(2)
Z	2	4
ρ_{calc}, g/cm^3	3.426	2.967
abs coeff, mm^{-1}	17.95	22.52
obsd reflcns[a]/ params	1747/63	1540/62
R1[a]/wR2 (all data)	0.031/0.070	0.036/0.065

[a] $I > 2\sigma(I)$.

Table 2. Selected Bond Distances (Å) and Angles (deg) for $(HO(CH_2)_2NH_3)_2PbI_4$[a]

Pb−I(1)$^{\#1}$	3.1790(10)	Pb−I(2)$^{\#3}$	3.2258(5)
Pb−I(1)	3.1790(10)	Pb−I(2)$^{\#1}$	3.2349(6)
Pb−I(2)$^{\#2}$	3.2258(5)	Pb−I(2)	3.2349(6)
C(1)−N	1.483(9)	C(1)−C(2)	1.489(11)
O−C(2)	1.413(8)		
I(1)$^{\#1}$−Pb−I(1)	180.000(17)	I(1)−Pb−I(2)$^{\#1}$	92.711(14)
I(1)$^{\#1}$−Pb−I(2)$^{\#2}$	90.137(15)	I(2)$^{\#3}$−Pb−I(2)	89.034(14)
I(1)−Pb−I(2)$^{\#2}$	89.863(15)	I(2)$^{\#2}$−Pb−I(2)	90.966(14)
I(2)$^{\#2}$−Pb−I(2)	180.0	I(1)−Pb−I(2)	87.289(14)
Pb$^{\#4}$−I(2)−Pb	159.836(18)		

[a] Equivalent positions: (#1) $-x+1, -y+1, -z+1$; (#2) $-x+3/2, y+1/2, -z+1$; (#3) $x-1/2, -y+1/2, z$; (#4) $-x+3/2, y-1/2, -z+1$.

Table 3. Selected Bond Distances (Å) and Angles (deg) for $(HO(CH_2)_2NH_3)_2PbBr_4$[a]

Pb−Br(2)$^{\#1}$	2.9892(7)	Pb−Br(1)$^{\#3}$	3.0158(6)
Pb−Br(2)	2.9892(7)	Pb−Br(1)$^{\#1}$	3.0490(6)
Pb−Br(1)$^{\#2}$	3.0158(6)	Pb−Br(1)	3.0490(6)
O−C(2)	1.403(8)	N−C(1)	1.414(9)
C(2)−C(1)	1.448(12)		
Br(2)$^{\#1}$−Pb−Br(2)	177.94(3)	Br(2)−Pb−Br(1)	88.697(18)
Br(1)$^{\#2}$−Pb−Br(1)$^{\#1}$	174.86(3)	Br(2)−Pb−Br(1)$^{\#1}$	89.771(18)
Br(2)$^{\#1}$−Pb−Br(1)$^{\#2}$	91.556(18)	Br(1)$^{\#2}$−Pb−Br(1)	91.030(8)
Br(2)−Pb−Br(1)$^{\#2}$	89.846(18)	Br(1)$^{\#2}$−Pb−Br(1)$^{\#3}$	94.10(3)
Br(1)$^{\#1}$−Pb−Br(1)	83.84(3)	Pb$^{\#4}$−Br(1)−Pb	171.85(3)

[a] Equivalent positions: (#1) $-x, y, -z+1/2$; (#2) $-x-1/2, y-1/2, z$; (#3) $x+1/2, y-1/2, -z+1/2$; (#4) $x-1/2, y+1/2, -z+1/2$.

(8) Mercier, N.; Riou, A. *Chem. Commun.* **2004**, *7*, 844.
(9) Xu, Z.; Mitzi, D. B.; Dimitrakopoulos, C. D.; Maxcy, K. R. *Inorg. Chem.* **2003**, *42*, 2031.
(10) Mitzi, D. B.; Dimitrakopoulos, C. D.; Kosbar, L. L. *Chem. Mater.* **2001**, *13*, 3728.
(11) $[(CH_3)_3NCH_2CH_2NH_3]SnI_4$ compound: Xu, Z.; Mitzi, D. B.; Medeiros, D. R. *Inorg. Chem.* **2003**, *42*, 1400.

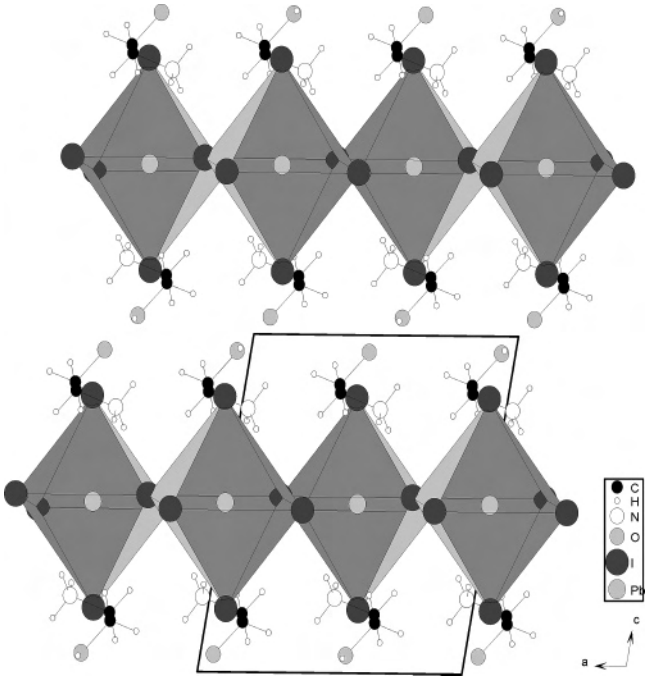

Figure 1. View of the layered hybrid perovskite structure of $(HO(CH_2)_2NH_3)_2PbI_4$. (PbI_6 octahedra are drawn in dark gray.)

determination of the high-temperature phase of $(HO(CH_2)_2NH_3)_2PbI_4$ was carried out using the TREOR program.[12]

Optical Properties. Absorption spectra were obtained on films using a Lambda 19 Perkin-Elmer spectrometer equipped with a Specac variable-temperature cell P/N 21525 (vacuum environment). Crystallized films could be prepared by the spin-coating technique for $(HO(CH_2)_2NH_3)_2PbI_4$ (solvent: acetonitrile) or by the drop cast method for $(HO(CH_2)_2NH_3)_2PbBr_4$ (solvent: dimethylformamide), the XRD patterns well demonstrating that the expected phases were only obtained.

Thermal Analysis. Thermogravimetric analysis (TGA) and differential scanning calorimetry (DSC) measurements were performed on the title compounds using TGA-2050 and DSC-2010 TA Instruments systems. TGA experiments consisted of a 10 °C/min ramp from 25 to 900 °C under a flowing nitrogen atmosphere, the platinum crucible containing approximately 15 mg of sample. DSC analysis were carried out by loading sample (approximately 5 mg) in a nearly hermetic aluminum capsule which was then located in the system unit (nitrogen atmosphere) and heated from room temperature up to 450 °C with a 10 °C/min ramp rate. For both compounds, cooling (5 °C/min ramp rate) was also performed after the first endothermic peak, assigned to a solid-state phase transition, to check the reversibility of this transition.

Results and Discussion

Crystal Structures. The crystal structure of $(HO(CH_2)_2NH_3)_2PbI_4$ is built up from sheets of corner-sharing PbI_6 octahedra alternating with organic cation layers (Figure 1). Two consecutive inorganic slabs appear slightly shifted one from each other, along *a*, and quite short interlayer iodine−iodine contacts are found, approximately along *c*, between apical iodines (see below). An interesting structural feature is that the $CH_2CH_2NH_3$ fragment approximately lies in the

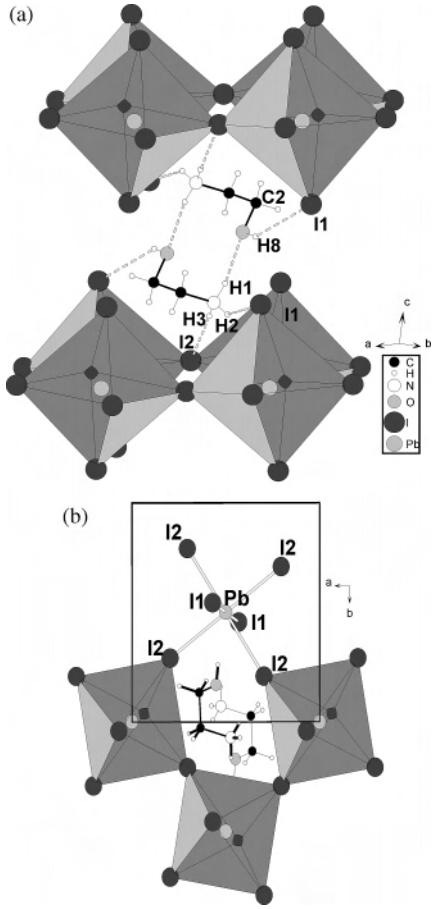

Figure 2. (a) Hydrogen bonding (dashed lines) between two adjacent ammonium cations and at the organic−inorganic interface in $(HO(CH_2)_2NH_3)_2PbI_4$. (b) View down along *c* of four adjacent centrosymmetrical PbI_6 octahedra together with cations located at each side of the inorganic sheet.

(*a*,*b*) planes at the elevation of the apical iodine atoms in any perovskite layer, with the hydroxyl groups only protruding out forward the interlayer space. This unusual situation is mainly due to the hydrogen bonding between two adjacent organic cations (Figure 2a). As encountered in such hybrids,[1,13] ammonium parts interact with the anionic inorganic network. However, only two of three hydrogen atoms of primary ammonium are here binded in H···I contacts (N−H3···I2, 2.92 Å; N−H2···I1, 2.86 Å), the third one being directed toward the oxygen atom belonging to the neighboring molecule (N−H1···O, 2.23 Å; Figure 2a). A symmetrical situation occurs for pairs of molecules, leading to a hydrogen-bond network defining cyclic motifs denoted $R_2^2(10)$ in Etter's notation.[14] These dimers are positioned in such a way that interactions between apical iodides and H atoms belonging to hydroxyl groups could also occur, the H1−O−H8 bond angle being 105.5° (Figure 2a). Finally, the hydrogen bonding both defines a pathway between adjacent perovskite layers and certainly brings these layers together, as illustrated by quite short interlayer I···I contacts, $d = 4.279(2)$ Å (even if this value is higher than the van der Waals distance (4.0 Å);[15] only one such hybrid based on group 14 metal halides has been reported with shorter contacts (4.19 Å)[11]).

(12) Werner, P. E.; Eriksson, L.; Westdahl, M. C. *J. Appl. Crystallogr.* **1985**, *18*, 367.
(13) Mitzi, D. B. *Chem. Mater.* **1996**, *8*, 791.
(14) Etter, M. C.; MacDonald, J. C. *Acta Crystallogr.* **1990**, *B46*, 256.
(15) Bondi, A. *J. Phys. Chem.* **1964**, *68*, 441.

The inorganic framework does not appear really distorted (Figure 2b): the centrosymmetrical PbI_6 unit geometry is close to the ideal octahedral geometry (Table 2), indicating minimal stereoactivity of 6s lone-pair electrons of lead atoms.[16] Pb and equatorial I atoms lie approximately in (*a*,*b*) planes, indicating no tilt of adjacent octahedra, and the Pb−I−Pb bond angle in equatorial PbI_2 planes is 159.8(1)°, a quite high value for such hybrids,[1,10,11] nevertheless lower than the one observed in a 2,2′-biimidazolium lead(II)−iodide compound (173.7°).[17] These interesting bonding features can be related in part both to the relative disposition of molecules and to a less strong hydrogen bonding between primary ammonium parts and PbI_4^{2-} layers (due to NH_3^+···OH interactions), compared to other known such hybrids.

The examination of the layered structure of $(HO(CH_2)_2NH_3)_2PbBr_4$ shows that identical $R_2^2(10)$ cyclic motifs defined by pairs of molecules are also encountered between the perovskite sheets. However, in $(HO(CH_2)_2NH_3)_2PbBr_4$, the conformation of molecules appears slightly different, with the CH_2OH part of molecules clearly out of the apical halide planes (Figure 3a), leading to a relative longer interlayer distance, and consequently precluding Br···Br contacts (d(Br···Br), 4.36(2) Å; $2R_{vdw}$(Br) = 3.70 Å).[15] On the other hand, the relative position of molecules located at each side of inorganic sheets, with only the CH_2NH_3 parts lying in the apical iodide planes, has a good impact on the equatorial Pb−Br−Pb bond angle (171.8°, Table 3): the perovskite layers appear only slightly distorted, four adjacent equatorial bromine atoms approximately defining a square (Figure 3b). By comparison, in the structure of $(HO(CH_2)_2NH_3)_2PbI_4$, four adjacent equatorial iodine atoms define a rhomb in which fit, on the projection, the molecules located on both sides of the sheet (Figure 2b). It is also interesting to note that a symmetry center is found in the PbI_2 equatorial planes of $(HO(CH_2)_2NH_3)_2PbI_4$ (Figure 2b), while this situation does not occur in $(HO(CH_2)_2NH_3)_2PbBr_4$ (Figure 3b). Finally, we notice that the incorporation of this noninnocent cation, involved in a unique hydrogen bonding, leads to two different structures of perovskites only differing in the nature of halide.

Phase Transition and Optical Properties. The observation of a color change of samples heated on a Köfler apparatus first revealed a probable solid-state phase transition: the bright orange colored powder of $(OH(CH_2)_2NH_3)_2PbI_4$ turned to pale orange/yellow above 100 °C, while the change from pale yellow to white occurred at approximately 130 °C for $(OH(CH_2)_2NH_3)_2PbBr_4$. To characterize the phase transitions, but also to examine the thermal stability of the title compounds, DSC measurements and TG analysis were carried out in the 20−450 and 20−900 °C ranges, respectively (see Experimental Section). For both perovskites, the DSC curve shows a first endothermic peak (96 °C for $(OH(CH_2)_2NH_3)_2PbI_4$; 125 °C for $(OH(CH_2)_2NH_3)_2PbBr_4$), which is assigned, in accordance with preliminary observations, to a structural transition. Then, the thermal behavior of both compounds comprises a melting transition (second endotherm) before the complete decomposition of $(OH(CH_2)_2NH_3)_2PbX_4$ (loss of 2 HX and 2 $OH(CH_2)_2NH_2$) and finally the evaporation of PbX_2 (see Supporting Information for X = I and Figure 4 for X = Br; theoretical weight loss percentages for the TG curve are 43.6 (observed: 43.75)

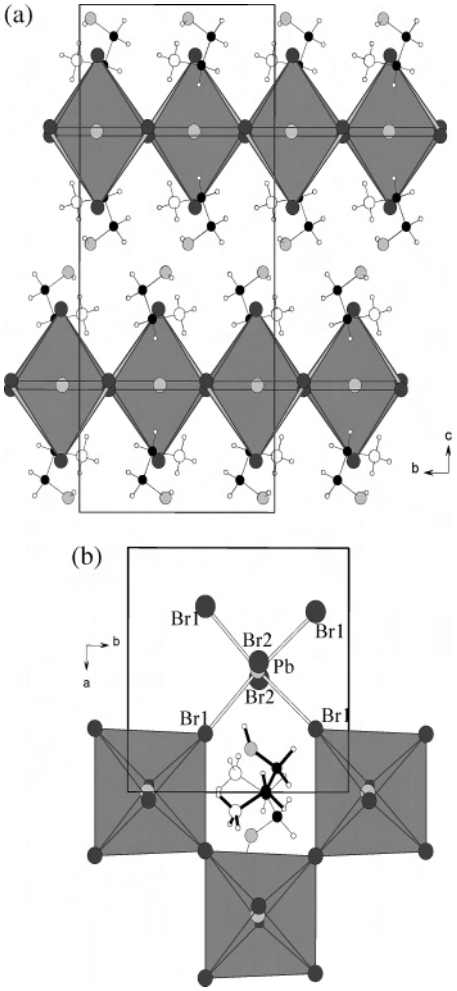

Figure 3. (a) View of the layered hybrid perovskite structure of $(HO(CH_2)_2NH_3)_2PbBr_4$. (b) View down along *c* of four adjacent $PbBr_6$ octahedra, together with cations located at each side of the inorganic sheet.

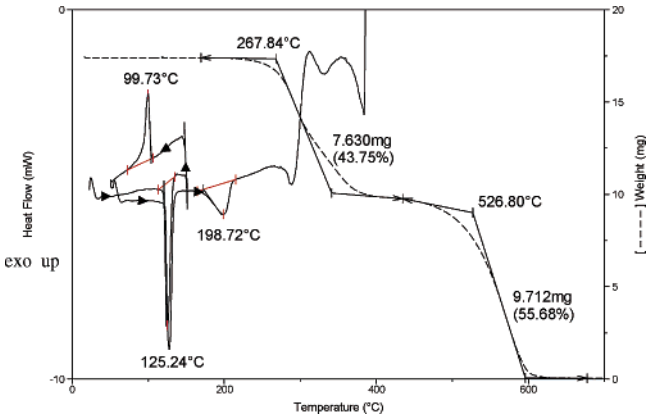

Figure 4. TGA and DSC scans (dashed and filled lines, respectively) for $(HO(CH_2)_2NH_3)_2PbBr_4$. The weight loss occurs in two steps corresponding to the decomposition of the salt and to the evaporation of $PbBr_2$. The DSC curve shows the reversibility of the structural phase transition (125 °C), before the endothermic melting transition (198 °C), and finally the decomposition.

(16) Donaldson, J. D.; Grimes, S. M. *Rev. Silicon, Germanium, Tin Lead Compd.* **1984**, *8*, 1.
(17) Tang, Z.; Guan, J.; Guloy, A. M. *J. Mater. Chem.* **2001**, *11*, 479.

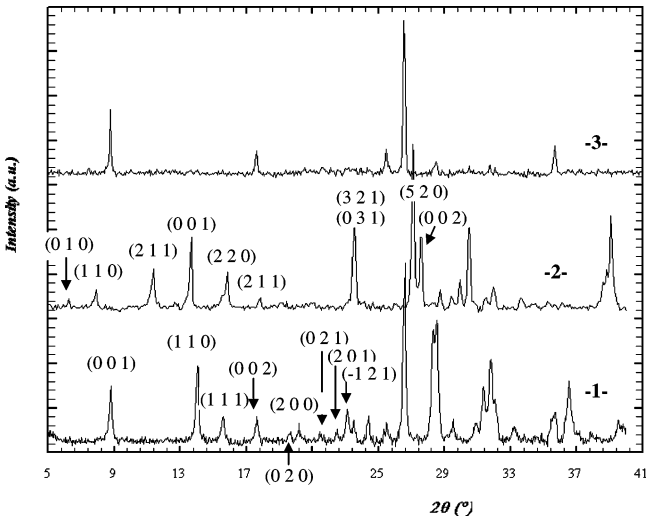

Figure 5. X-ray diffraction patterns of $(HO(CH_2)_2NH_3)_2PbI_4$, 1, at room temperature, 2, immediately after an annealing at 130 °C during 12 h, and, 3, 40 h after its annealing at 130 °C, together with the indexation of the first peaks in the monoclinic cell (a = 8.935(1) Å, b = 9.056(2) Å, c = 10.214(3) Å, β = 100.26(1)°) and the orthorhombic cell (a_{HT} = 18.567(6) Å, b_{HT} = 13.833(6) Å, c_{HT} = 6.437(2) Å) of the room-temperature phase (1) and the high-temperature phase (2), respectively.

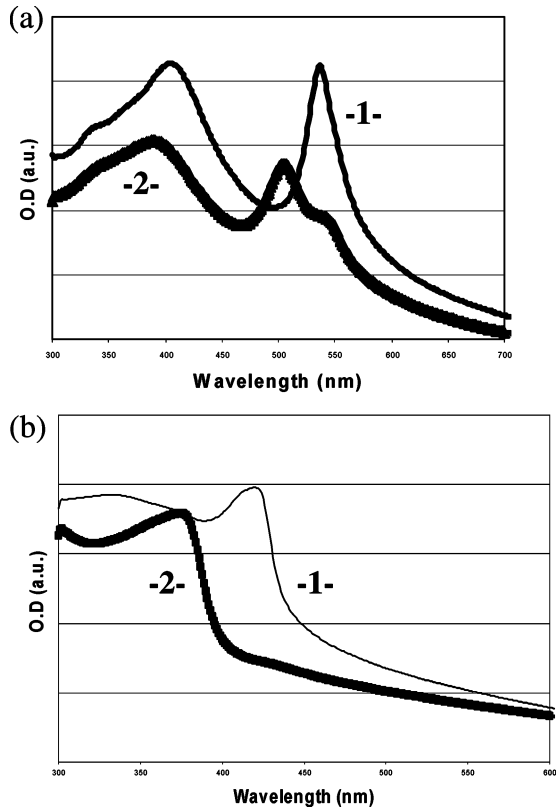

Figure 6. UV−vis spectra of a film of (a) $(HO(CH_2)_2NH_3)_2PbI_4$ (300−700 nm range; 1, at room temperature; 2, at 100 °C) and (b) $(HO(CH_2)_2NH_3)_2PbBr_4$ (300−600 nm range; 1, at room temperature; 2, at 140 °C).

and 56.4 (55.68)). Figure 4 also shows the reversibility of the phase transition in $(OH(CH_2)_2NH_3)_2PbBr_4$ by ramping up and down in temperature through the corresponding endotherm of the DSC curve. This reversible phenomenon could also be visually verified by the color change, from white to pale yellow, as soon as the sample is cooled below 100 °C. In the case of $(OH(CH_2)_2NH_3)_2PbI_4$, the powder recovers its initial color after a few hours left at room temperature. This slow phenomenon allowed us to perform a 40 min room-temperature X-ray powder scan of the high temperature phase immediately after its annealing to 130 °C (Figure 5, curve 2), while the reversibility of the transition could be checked from a X-ray pattern carried out 40 h after the annealing at 130 °C (Figure 5, curve 3). It must be noted that the missing reflections in curve 3, compared to curve 1 (X-ray pattern of sample before annealing), is assigned to a preferred orientation upon annealing. An orthorhombic cell of the high-temperature (HT) phase of $(OH(CH_2)_2NH_3)_2PbI_4$ is proposed from the 25 first lines of the X-ray powder pattern (TREOR factor $M(20)$ = 13; results given as Supporting Information), with a_{HT} = 18.567(6) Å, b_{HT} = 13.833(6) Å, c_{HT} = 6.437(2) Å, and V_{HT} = 1653 Å^3. This cell hypothesis seems plausible, first because the volume of the high-temperature phase appears just greater than twice the volume of the room temperature phase and second owing to the relationships between the a_{HT} and c_{HT} parameters and the a and b parameters of the room-temperature phase: $\vec{a}_{HT} = 3/2(\vec{a} + \vec{b})$ and $\vec{c}_{HT} = 1/2(\vec{a} - \vec{b})$, respectively. Note that c_{HT} corresponds to two Pb−I distances and that a_{HT} is approximately three times c_{HT}. A change in the hydrogen bonding probably occurs, with molecules standing up in the interlayer space and OH parts interacting together, leading to an increase of the interlayer distance, from approximately d = 10.20 Å (c parameter of the room-temperature phase) to d = 13.83 Å (b_{HT} parameter). This last value is comparable to the one observed in $(C_3H_7NH_3)_2MnCl_4$ (d = 12.97 Å),[18] taking account of the similar molecular length of both 2-hydroxyethylammonium and propylammonium cation and of the change of halide, from chloride in $(C_3H_7NH_3)_2MnCl_4$ to iodide in $(HO(CH_2)_2NH_3)_2PbI_4$. Finally, this would lead to a more conventional situation for ammonium groups, no I···I interlayer contacts, and probably a more distorted perovskite layer.

Such hybrid materials have an exciton state, associated with the band gap of the inorganic layers, in their electronic structure, giving a sharp peak in the corresponding optical absorption spectra even at room temperature.[19,20] Also, the shifts of these characteristic peaks reflect a change in the electronic structure of hybrids, which is strongly related to the bonding features of the perovskite layers. The UV−vis absorption spectra of films of $(OH(CH_2)_2NH_3)_2PbX_4$ (X = I, Br) at room temperature and 120 °C (X = I) or 140 °C (X = Br) are shown in Figure 6. The absorption spectra of the room-temperature phases display an exciton peak at 536 nm (2.31 eV, X = I) and 417 nm (2.97 eV, X = Br). These wavelengths are, to our knowledge, the highest values observed for PbX_4-based (X = I, Br) perovskites (reduced band gap). This reveals a good impact of organic cations involved in unique interactions at the interface on the bonding features of the perovskite layers, as already underlined in

(18) Peterson, E. R.; Willet, R. D. *J. Chem. Phys.* **1972**, *56*, 1879.
(19) Ishihara, T.; Takahashi, J.; Goto, T. *Solid State Commun.* **1989**, *69*, 933.
(20) Hong, X.; Ishihara, T.; Nurmikko, A. V. *Phys. Rev. B* **1992**, *45*, 6961.

the structural part. A blue shift of the exciton peak to 504 nm (2.46 eV, X = I) or to 374 nm (3.32 eV, X = Br) occurs in the absorption spectra of the high-temperature (HT) phases (Figure 6, curves 2). For HT-$(OH(CH_2)_2NH_3)_2PbI_4$, $\lambda = 504$ nm well fits in the range of usually observed values for such hybrids (500−515 nm region),[2a−b,7b,14,21] which correlates with the structural study. For HT-$(OH(CH_2)_2NH_3)_2PbBr_4$, $\lambda = 374$ nm appears low compared to other $PbBr_4^{2-}$-based perovkites (λ in the range 390−406 nm),[1,2b,21a] certainly revealing very distorted perovskite layers. A few structural transitions in hybrid perovskites based on long-chain alkylammonium have been studied in the past and are discussed in a recent review.[1] These transitions, which are order−disorder transitions or due to either a conformation change or a melting of alkyl chains, do not strongly affect the inorganic frameworks, except in $(C_{10}H_{21}NH_3)_2PbI_4$, where consequently a substantial change of the exciton peak energy (0.15 eV) is observed.[19] In both title compounds, the significant change of the exciton peak energy (0.15 eV (X = I); 0.35 eV (X = Br)) shows that perovskite layers of the room-temperature and high-temperature phases display very different bonding features. This can be assigned to the hydroxyl groups of organic cations able to be involved in hydrogen bonding at the interface (room-temperature phase, slight distortion of perovskite layers) or (certainly) in the interlayer space (high-temperature phase, distorted inorganic sheets).

Conclusion

In summary, a unique hydrogen-bonding network is created between inorganic layers of the hybrid perovskites $(HO(CH_2)_2NH_3)_2PbX_4$ (X = I, Br) using the 2-hydroxyethylammonium cations. The resultant structural features as weaker interactions between primary ammonium and PbX_4^{2-} layers, interlayer X···X contacts (X = I compound), or interesting bonding characteristics of the inorganic framework explain the reduced band gaps of these salts, as illustrated by their exciton peak at $\lambda_{exc} = 536$ nm (X = I) and $\lambda_{exc} = 417$ nm (X = Br). We may also speculate that the hydrogen bonding can provide a channel for stronger electronic coupling between perovskite sheets, also contributing to the reduction of band gap.

A change in the hydrogen bonding at 96 °C (X = I) or at 125 °C (X = Br) is proposed to explain the color change together with a significant blue shift of the exciton peak to $\lambda_{exc} = 504$ nm (X = I) or $\lambda_{exc} = 374$ nm (X = Br) during a (reversible) structural transition. This demonstrates the possibility, using such bifunctional cations able to strongly influence the bonding features of the inorganic framework, to effectively tune electronic properties of hybrid perovskites under a change of temperature or pressure.

Supporting Information Available: Full crystallographic data in CIF format, complete tables of bond distances and atomic coordinates, a checkCIF report, powder X-ray diffraction patterns of the room-temperature phases of $(HO(CH_2)_2NH_3)_2PbX_4$ (X = I, Br) with complete indexation, results of the cell determination of the high-temperature phase of $(HO(CH_2)_2NH_3)_2PbI_4$, and TGA and DSC scans for $(HO(CH_2)_2NH_3)_2PbI_4$. This material is available free of charge via the Internet at http://pubs.acs.org.

IC048814U

(21) (a) Papavassiliou, G. C.; Koutselas, I. B. *Synth. Met.* **1995**, *71*, 1713. (b) Papavassiliou, G. C.; Mousdis, G. A.; Raptopoulo; C. P.; Terzis, A. *Z. Naturforsch.* **1999**, *54b*, 1405.